J. Fluid Mech. (2003), *vol.* 495, *pp.* 19–33.
DOI: 10.1017/S0022112003006062 Printed in the United Kingdom

Self-organization of decaying quasi-two-dimensional turbulence in stratified fluid in rectangular containers

By S. R. MAASSEN, H. J. H. CLERCX AND G. J. F. VAN HEIJST

Fluid Dynamics Laboratory, Department of Physics, Eindhoven University of Technology, PO Box 513, 5600 MB Eindhoven, The Netherlands

(Received 26 November 2002 and in revised form 2 June 2003)

Laboratory experiments on decaying quasi-two-dimensional turbulence have been performed in stratified fluid inside containers with length-to-width ratios δ up to 5. The Reynolds number Re of the horizontal flow, based on the r.m.s. velocity of the initial flow field and the half-width H of the container, was typically between 1000 and 3000. The turbulence was generated by towing an array of vertical cylinders through the container which was filled with a two-layer stratified fluid. By varying the grid configuration a different amount of angular momentum could be added to the initial flow. The evolution of the flow was visualized by two-dimensional particle tracking velocimetry. The observed decay has been investigated with the emphasis on the final states as function of δ, Re and the angular momentum initially added to the flow. In addition, numerical simulations were carried out for decaying two-dimensional turbulence on rectangular domains with $\delta = 2$ and 3. In these runs zero net angular momentum was added to the initial flow field. The numerical study focused on the final states as a function of δ and Re. The numerically obtained final states appeared to agree with the experimental observations. Furthermore, they indicate a clear difference between the predictions of quasi-stationary final states from statistical-mechanical theories and the final states as found in the numerical simulations.

1. Introduction

Previous experimental and numerical studies of decaying two-dimensional turbulence in square and circular domains with no-slip (or, for numerical simulations, stress-free) boundaries by Li & Montgomery (1996), Li, Montgomery & Jones (1996, 1997), Clercx, Maassen & van Heijst (1998, 1999) and Maassen, Clercx & van Heijst (2002) revealed the important role the type of boundary conditions plays in the decay process. In particular, decay with no-slip boundary conditions is relevant, and differs considerably from decay with stress-free boundary conditions. The most frequently observed quasi-stationary final state in these experiments and simulations is a domain-filling cell. This final state is observed for the circular domain (with non-zero net angular momentum added to the initial flow) by Li *et al.* (1996) and Maassen *et al.* (2002), and for the square domain (regardless of the amount of net angular momentum added to the initial flow) by Clercx *et al.* (1998, 1999) and Maassen *et al.* (2002). The role of the non-zero net angular momentum added to the initial flow in the decay of (quasi-)two-dimensional turbulence seems to be an

acceleration of the self-organization process. Finally, a dipolar structure is found for decaying two-dimensional turbulence in a circular domain (with zero net angular momentum added to the initial flow) by Li *et al.* (1996, 1997) and Maassen *et al.* (2002).

In the present experiments on decaying quasi-two-dimensional turbulence in rectangular containers, an initially small-scale, disordered (quasi-)two-dimensional flow, generated by forcing the fluid with a grid of vertical rods, organizes into a linear array of vortex cells with alternating circulations. This phenomenon itself is not new: it was observed by van Heijst, Davies & Davis (1990), van de Konijnenberg *et al.* (1994) and Flór (1994), in laboratory experiments on spin-up phenomena and on decaying stably stratified flow in rectangular containers. However, these experimental studies concern decay processes from an initial two-dimensional flow field possessing either large-scale symmetries or a large amount of angular momentum (with respect to the centre of the container). In the experiments by Flór (1994), two different types of forcing were used to create an initial flow field. In one type of experiment, the fluid was forced by two oppositely positioned jets mounted on the longer sidewalls of the container. For moderate aspect ratios ($\delta \leqslant 3$) these jets gave rise to one large initial circulation cell, with a size comparable to the length of the longer side of the container. For larger aspect ratios ($\delta \geqslant 4$) two large circulation cells with sizes comparable to the half-length of the longer side were formed during the forcing. In both cases, the initial circulation cells were observed to organize into an array of smaller, almost circular vortices, with sizes comparable to the smaller side of the container. Alternatively, an initially small-scale flow was created by stirring the fluid with a rake (by hand), and a cell pattern of vortices with sizes comparable to the smaller side of the container was formed due to self-organization of decaying quasi-two-dimensional turbulence. A similar phenomenon has been observed during the spin-up of a non-stratified fluid in a rectangular container (van Heijst *et al.* 1990; van de Konijnenberg *et al.* 1994), in which the flow is approximately two-dimensional due to the presence of a uniform background rotation. In these experiments, the angular velocity of a steadily rotating container was suddenly increased to a new constant value. The adjustment of the fluid inside the container to this new angular velocity is characterized by the formation of a cellular pattern that fills the entire flow domain. In both types of experiment the number of vortices in the final cell pattern is approximately equal to the aspect ratio δ of the container.

The aim of the present investigation is to gain a deeper understanding of the cell pattern formation in decaying quasi-two-dimensional turbulence in rectangular containers with $\delta \neq 1$, as was observed in the rake-forced experiments. Since no symmetry or large-scale motion is introduced to the flow initially, the evolution towards a final cell pattern in these experiments is less clear and predictable than in jet-forced flow in a stratified fluid or in spin-up experiments. In particular, we focus on the role of the angular momentum of the initial flow field, which can be controlled in the experiments (see § 3). In all previous experiments the initial two-dimensional flow field contained angular momentum, but its role in the decay process was completely ignored (except for the spin-up experiments). An important question is: how will the decay process be modified when the initial flow field does not contain angular momentum?

The organization of this paper is as follows. In § 2 a brief outline of the experimental technique is given. The results of laboratory experiments on decaying stably stratified turbulence in containers with different aspect ratios ($\delta = 2$, 3, 4, and 5) are presented in § 3. A discussion of this study and conclusion are presented in § 4.

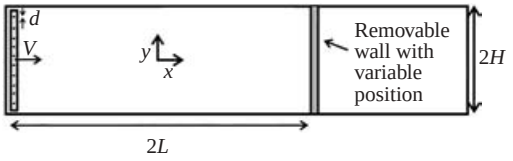

FIGURE 1. Top view of the experimental configuration for a rectangular domain with aspect ratio $\delta = L/H$. A grid of cylindrical rods (each with a diameter d) is moved with constant speed V along the x-axis, from one side of the domain to the other side.

2. Experimental set-up

The laboratory experiments presented in this section were performed in a rectangular Perspex container with horizontal dimensions $200 \times 40\ \mathrm{cm}^2$. The horizontal dimensions of the actual working flow domain were determined by the position of a removable Perspex wall mounted between the two longer sides of the container (see figure 1). In this way, the aspect ratio δ, defined as the ratio between length and width of the working flow domain, could be varied. Apart from the geometry of the container, the experimental equipment used in the present experiments is similar to the set-up used for experiments in circular and square containers described by Maassen (2000) and Maassen *et al.* (2002). Therefore, we give here only a concise description of the experimental procedure and discuss only briefly the typical behaviour of decaying stratified flow.

The whole container (that is, the two regions on either side of the removable wall) is filled with a two-layer fluid, consisting of a layer of salty water at the bottom (with a density $\rho_2 \approx 1.1\ \mathrm{g\,cm^{-3}}$) and a layer of fresh water on top (density $\rho_1 \approx 1.0\ \mathrm{g\,cm^{-3}}$), both with a thickness of approximately 10 cm. Due to molecular diffusion of salt and to mixing of the two fluids introduced during the filling of the container, a linearly stratified interfacial layer is established at the interface between the fresh and the salty fluid layers. The thickness of this interfacial layer varies from a few centimetres immediately after the container is filled, to approximately 10 cm after a few days. Therefore, the buoyancy frequency within this layer, defined as

$$N^2 = -\frac{g}{\rho_0}\frac{\rho_1 - \rho_2}{h}, \tag{2.1}$$

with g the gravitational acceleration, h the thickness of the interfacial layer and $\rho_0 = (\rho_1 + \rho_2)/2$ the average density within this layer, varies between $N = 4\ \mathrm{rad\,s^{-1}}$ and $N = 2.5\ \mathrm{rad\,s^{-1}}$.

At the start of each experiment, a small-scale, disordered flow field is generated in the fluid by moving a grid of vertical bars (each with a diameter $d = 3\ \mathrm{mm}$) parallel to the longer sides of the container (see figure 1). A detailed description of this forcing mechanism can be found in Maassen *et al.* (2002). After the grid has reached the opposite side of the domain, it is lifted out of the fluid by hand. During the forcing, many small-scale vortices emerge in the wake behind the moving vertical bars. Thus, an initially three-dimensional turbulent flow is generated in the two unstratified layers as well as in the linearly stratified interfacial layer. However, in the unstratified layers these three-dimensional motions damp out quickly, whereas the motion in the stratified interfacial layer collapses to a planar, quasi-two-dimensional flow, which shows a much slower decay. This collapse from three-dimensional to quasi-two-dimensional flow in the interface is accompanied by the generation of internal waves. A more extensive discussion of the vertical collapse and internal wave

generation in stratified turbulence is presented by Riley, Metcalfe & Weissman (1981), Lilly (1983) and Riley & Lelong (2000).

To visualize and quantify the quasi-two-dimensional flow in the interfacial layer, the fluid is seeded with small polystyrene particles with density $\rho \approx 1.04\,\mathrm{g\,cm^{-3}}$ and a typical size of 1 mm. The motion of these particles is monitored by a video camera mounted at some distance above the container and recorded on a video tape. After the experiments, instantaneous velocity fields are determined by means of particle tracking velocimetry (PTV). In order to obtain additional information on the flow field, such as contour plots of the vorticity field, the stream function and the Weiss function (see Weiss 1981), the non-gridded vector fields obtained by PTV are interpolated to a grid of 40×40 grid points by using a cubic spline interpolation method (for details, see Nguyen Duc & Sommeria 1988), and subsequently fitted with a doubly truncated series of Chebyshev polynomials. The Chebyshev fitting procedure has primarily been introduced to improve the computation of the vorticity field from the PTV data (see Maassen 2000). The total errors in the velocity field, introduced by PTV and the post-processing procedure, are estimated to be on the order of 10%.

The Reynolds number of the experiments is defined as $Re^* = HU/\nu$, with H the half-width of the short sidewall of the container†, U the root-mean-square velocity of the initial flow field, and ν the kinematic viscosity of water. All variables are made dimensionless using the length scale H and the eddy-turnover time H/U. In the present experiments, the Reynolds number Re^* varied between $Re^* \approx 1000$ and $Re^* \approx 3000$. However, due to strong vertical shearing in the stratified interface, dissipation of kinetic energy in the experiments is much stronger than in numerical simulations of purely two-dimensional decaying turbulence with no-slip boundaries and comparable Reynolds numbers (see Yap & Van Atta 1993; Fincham, Maxworthy & Spedding 1996; Maassen *et al.* 2002). Therefore, the actual effective Reynolds number of the present experiments is lower than Re^*. A detailed comparison for the square-container case has been discussed by Maassen *et al.* (2002). There it was found that $Re \approx 0.4Re^*$.

An analysis of the role of vertical shearing, the influence of the strength of the stratification, and the different behaviour of decaying quasi-two-dimensional flows in linearly stratified and two-layer fluids has been omitted for the present experiments. These issues have been considered for the experiments in square and circular containers as reported by Maassen *et al.* (2002). These experiments revealed that the quasi-two-dimensional motions in the centre of the linearly stratified interfacial layer are shielded from the (almost motionless) unstratified layers above and beneath the interface. In agreement with the observations made by Yap & Van Atta (1993), the dissipation of kinetic energy is more effective in experiments with a stronger stratification, while the dissipation of enstrophy ($\Omega = \frac{1}{2}\int \omega^2 \,\mathrm{d}A$, with ω the vorticity) seems to be unaffected by the strength of the stratification. These experiments also reveal that approximately 80% of the total dissipation is due to vertical shearing of the horizontal velocity, and the remaining 20% is due to horizontal strain (in agreement with observations by Fincham *et al.* 1996). It is anticipated that these conclusions also hold for the present experiments in rectangular containers where a similar experimental set-up has been used.

† The present investigation is focused on the evolution of the randomly disturbed flow to an array of vortices with a characteristic radius H, and not on the small-scale details of the forcing. Therefore, we prefer the width of the container over the mesh size of the rake as the characteristic length scale in our (numerical) experiments.

Label	δ	T_b	Grid	V (cm s^{-1})	Re^*	Shown in figure:
1	2	0.09	R4	15	1000	3
2	2	0	R1	15	1500	5
3	2	0.01	R5	15	1000	4
4	3	0	R2	20	3000	6
5	3	0.09	R4	30	1500	–
6	4	0	R3	20	3000	–

TABLE 1. Characteristic parameters corresponding to the experiments plotted in figure 2, performed in rectangular containers with aspect ratio δ. The numbers in the first column correspond to the labels in figure 2. The parameter T_b denotes the normalized dimensionless torque of the drag forces exerted on the grid during the forcing (defined in equation 3.1), V is the speed of the grid and Re^* the Reynolds number of the initial flow field. The grid configurations (fourth column) are specified in the Appendix.

3. Laboratory experiments

During the initial forcing, a drag force is exerted by the fluid on each of the rods in the moving grid. In about half of the experiments, the rods in the grid were arranged in such a way that this drag force did not induce a net torque with respect to the centre of the flow domain. This type of experiment is referred to as 'unbiased'. In the other experiments, the rods were arranged in such a way that the net torque induced by the drag force was not zero, and therefore the grid introduced a slight 'bias' to the initial flow. This bias resulted in a net large-scale motion superimposed on the small vortices emerging in the wake of the grid. The bias in the initial forcing is measured in terms of the normalized dimensionless torque T_b per rod with respect to the line $x = 0$ (see figure 1), defined as

$$T_b = \frac{|T|}{N_r F_D H}, \tag{3.1}$$

with F_D the drag force exerted by the fluid on one rod ($F_D = \frac{1}{2} C_D \rho V^2 l d$, with the drag coefficient C_D obtained from experimental data (see Blevins 1984), ρ the fluid density, V the speed of the cylindrical rod, l the length and d the diameter of the rod), N_r the number of rods in the grid, H the half-width of the domain and T the net torque obtained by adding up the contributions $F_D y$ of all rods. (Note that the contribution to T of a rod at position y exactly cancels the contribution of a rod at position $-y$). The present experiments were carried out with $T_b = 0$, $T_b = 0.01$ or $T_b = 0.09$. Here, the dimensionless torque is not used as a similarity parameter for collapsing data from many different experiments, but is only used to produce (and to make a distinction between) 'biased' and 'unbiased' initial turbulent flows. The grid configurations used to generate these values of T_b are listed in table 1 (fourth column) and specified in the Appendix. We remark that a certain translation speed V resulted in a lower value of Re^* for experiments with $T_b \neq 0$ than for experiments with $T_b = 0$ (see table 1).

Several experiments were performed for $\delta = 2$, 3, 4 and 5 with Reynolds numbers in the range $Re^* \approx 1000$–3000. The decay of kinetic energy in these particular experiments is plotted in figure 2. The characteristic parameters corresponding to the labels in this figure are indicated in table 1. The data in figure 2 suggest that the dissipation of kinetic energy is stronger in experiments with $\delta = 2$ than in experiments with $\delta = 3$ or $\delta = 4$ (no such data could be obtained for experiments with $\delta = 5$). The data in figure 2 also suggest a reduced dissipation of kinetic energy when a substantial

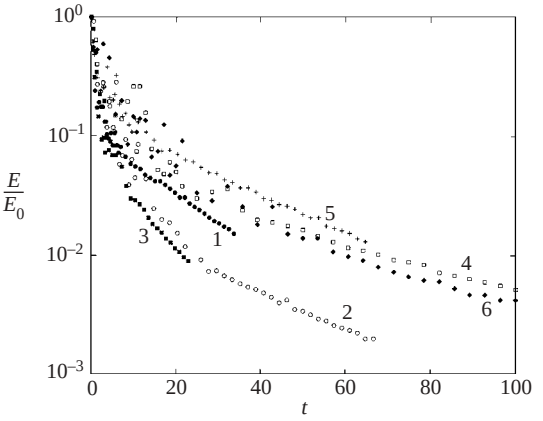

FIGURE 2. Normalized kinetic energy E/E_0 plotted logarithmically versus time for the experiments performed in containers with aspect ratio $\delta \neq 1$ that are explicitly shown in this section. The parameters corresponding to these experiments are listed in table 1.

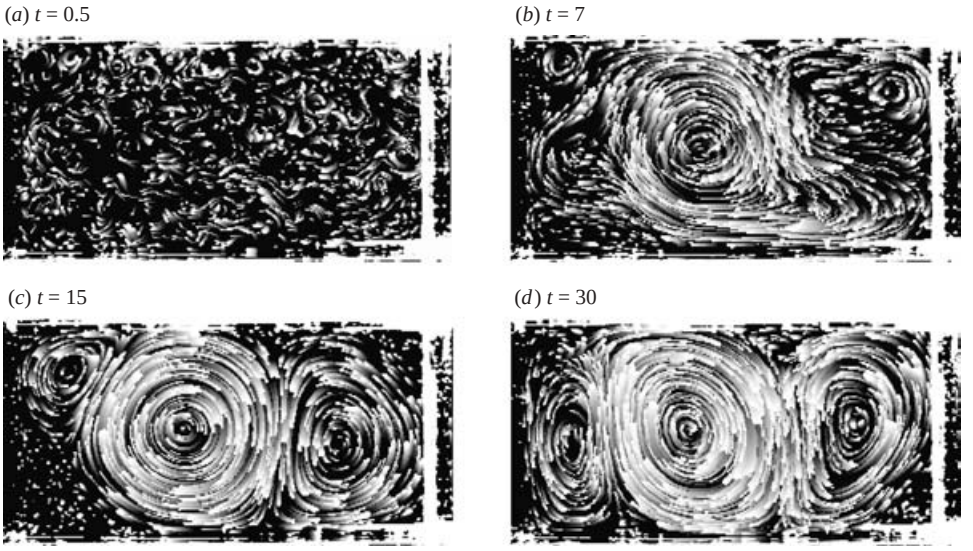

FIGURE 3. Streak images of an experiment performed in a container with aspect ratio $\delta = 2$, $Re^* = 1000$ and a small bias in the initial forcing ($T_b = 0.09$). The tails of the streaks represent the displacements of tracer particles during an interval of (*a*) 0.1, (*b*) 2.5 and (*c*, *d*) 5 dimensionless time units.

bias ($T_b = 0.09$) is present. Plotting the same data on a doubly logarithmic graph reveals that these differences occur during the first 10 dimensionless time units. For $t \geqslant 10$ all curves can be fitted with the power law $E \propto t^{-1.5 \pm 0.2}$ in agreement with previous findings on decaying quasi-two-dimensional turbulence in stratified fluids with similar buoyancy frequencies by Fincham *et al.* (1996) and Maassen *et al.* (2002). In all experiments (either biased or unbiased), small quasi-two-dimensional vortices emerge in the interfacial layer after the collapse from three-dimensional to quasi-two-dimensional turbulence. These vortices immediately start to organize into larger structures, and finally form a large-scale cell pattern that fills the whole flow domain. This process is clearly illustrated by the streak images plotted in figure 3 for an

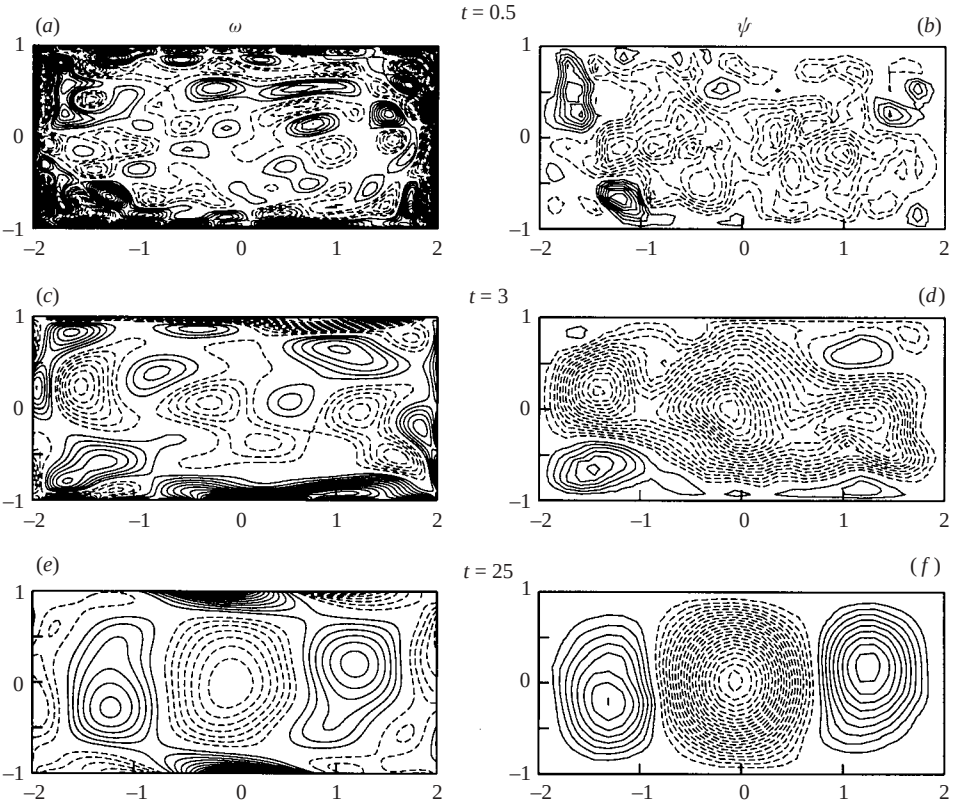

FIGURE 4. Vorticity (left column) and stream function (right column) contour plots of an experiment performed in a container with aspect ratio $\delta = 2$, $T_b = 0.01$ and $Re^* = 1000$. Dashed contours represent negative and solid contours represent positive values of the vorticity and the stream function. The contour level increment for the vorticity is (*a*) 3, (*c*) 0.5 and (*e*) 0.1, and for the stream function: (*b*) 0.04, (*d*) 0.012 and (*f*) 0.005.

experiment performed in a domain with $\delta = 2$. The streaks are produced by the PTV software, which displays the positions of tracer particles during a certain prescribed time interval. The length of each streak corresponds to the displacement of a particle during this time interval.

(i) $\delta = 2$

In the first experiment, shown in figure 3, the initial forcing was carried out with a bias $T_b = 0.09$. This bias results in a large-scale clockwise circulation at $t \simeq 3.5$, which forms a strong central vortex at $t \simeq 7$ (figure 3*b*). The final flow pattern in this experiment consists of three counter-rotating vortices (figure 3*c*, *d*): the strong vortex in the centre of the domain rotates in a clockwise direction; the two other (weaker) vortices rotate in the anti-clockwise direction. This process is visible more clearly in figure 4, where we have plotted some contours of vorticity (left column) and stream function (right column), for another experiment with $\delta = 2$ and biased forcing ($T_b = 0.01$). In these figures, the presence of a large-scale motion in the initial stage of the evolution is particularly clearly visible in the stream function plots (figure 4*b*, *d*). Together with the vorticity contour plots shown in figure 4(*a*, *c*), where many small vortices are visible, this observation indicates that this 'bias' is superimposed on the

	$\delta=2$			$\delta=3$			$\delta=4$			$\delta=5$		
Total number of experiments:	13			12			11			11		
Number of vortices in final state:	1^+	2	3	3	4	5	$4+1$	5	6	5	6	7
Number of experiments with $T_b=0$:	2	3	1	4	1	2	1	2	1	3	2	1
Number of experiments with $T_b\neq 0$:	2	0	5	2	3	0	4	3	0	3	2	0

TABLE 2. Characteristic parameters of the final states observed in experiments that were performed in rectangular containers with aspect ratio δ.

small vortices emerging in the wake of the grid. In this particular experiment, the large-scale motion results in the formation of three negative vortices at $t \approx 3$, which merge into one central vortex at $t \approx 15$. Meanwhile, positive vorticity is created in the lower left and upper right corners of the domain. These vorticity patches are advected by the central vortex into the interior of the domain, resulting in the formation of two positive vortices in the left and right parts of the domain (figure 4*e*). The formation of a large central vortex together with two wall-generated vortices of opposite sign is generic for all experiments with $\delta = 2$ in which a small bias was introduced to the fluid during the forcing. This behaviour is similar to the cell pattern formation observed in jet-forced experiments in stably stratified flow (Flór 1994) and in spin-up experiments (van Heijst *et al.* 1990). Since the forcing in these two cases is symmetric with respect to the centre of the container, the number of vortices in the final cell pattern is always odd. In most of the present experiments, the pattern formation was less 'symmetric' than in the experiment shown in figure 4. For example, in figure 3(*b–d*) the vortex emerging on the left of the strong vortex is much weaker than the vortex emerging in the right of the domain.

In table 2 we list the number of vortices in the final cell patterns that are observed in experiments with different values of δ, together with the number of biased and unbiased experiments in which these specific flow patterns were formed. This table indicates that, for the experiments with $\delta = 2$, a pattern of three vortices was formed in almost all experiments with biased forcing. In two experiments, the flow was dominated by one large vortex, accompanied by two vortices of opposite sign, with sizes much smaller than the width of the domain. The number of vortices in this latter flow pattern is indicated as 1^+.

In the experiment shown in figure 5, the initial forcing was unbiased ($T_b = 0$). In this case, no large-scale rotation is observed after the initial forcing, and two negative and two positive vortices are formed at $t \simeq 10$ (figure 5*a*). However, the two positive vortices start to rotate around the (strongest) negative vortex on the right of the domain at $t \simeq 20$ (figure 5*c*), thus forming a rotating tripolar structure, and are finally torn apart. This process can be understood by considering the Weiss function $Q = S^2 - \omega^2$ with ω the vorticity and S a measure of the rate of strain in a particular area of the flow (see Weiss 1981). The Weiss function for the same experiment (figure 5, right column) shows that the cores of the four vortices developing at $t \simeq 10$ are characterized by regions with negative values of Q, which are rotation-dominated or elliptic. The strain-dominated or hyperbolic regions ($Q > 0$) develop between the (stronger) negative vortex and the boundaries of the domain at $t \simeq 10$. Since the elliptic cores of the two weaker positive vortices are surrounded by a much larger hyperbolic area, these small vortices are advected in a clockwise direction around the negative vortex (thus forming an intermediate tripolar structure) and are finally

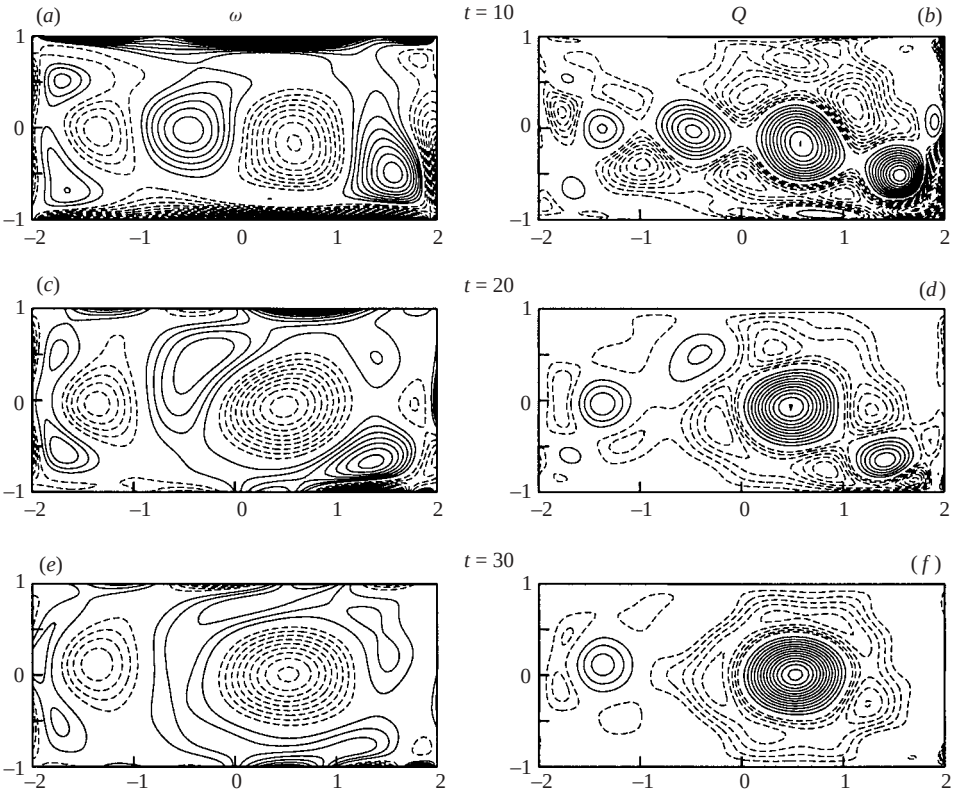

FIGURE 5. Vorticity (left column) and Weiss function (right column) contour plots of an experiment performed in a container with $\delta = 2$, $T_b = 0$ and $Re^* = 1500$. Left column: dashed contours represent negative values of vorticity and solid contours represent positive values. The contour level increment is (*a*) 0.2, (*c*) 0.15 and (*e*) 0.1. Right column: dashed contours represent hyperbolic regions ($Q > 0$) and solid contours represent elliptic regions ($Q < 0$). The contour level increment is (*b*) 0.15, (*d*) 0.08 and (*f*) 0.04 for the dashed contours and (*b*) 0.3, (*d*) 0.15 and (*f*) 0.08 for the solid contours.

torn apart by this vortex. The formation of a rotating tripole is observed in almost all unbiased experiments and simulations with $\delta = 2$ and no-slip boundaries (see also § 4)†.

(ii) $\delta = 3$

The influence of an initial bias is slightly different in experiments performed in a domain with $\delta = 3$. As can be inferred from table 2, the final patterns in these experiments consist of three or four vortices in the biased experiments ($T_b = 0.09$) and three, four or five vortices in the unbiased experiments ($T_b = 0$). In the case of unbiased forcing, the number of vortices in the final state depends, as was found for $\delta = 2$, on the random position of one or two strong vortices in the earlier stages of

† The term 'tripole' refers to a vortex consisting of one large core accompanied by two smaller and weaker satellites. The two satellites are not counted in the number of vortices of the final cell pattern indicated in table 2. The tripolar structure should not be confused with a cell pattern consisting of three vortices of more or less equal size and strength.

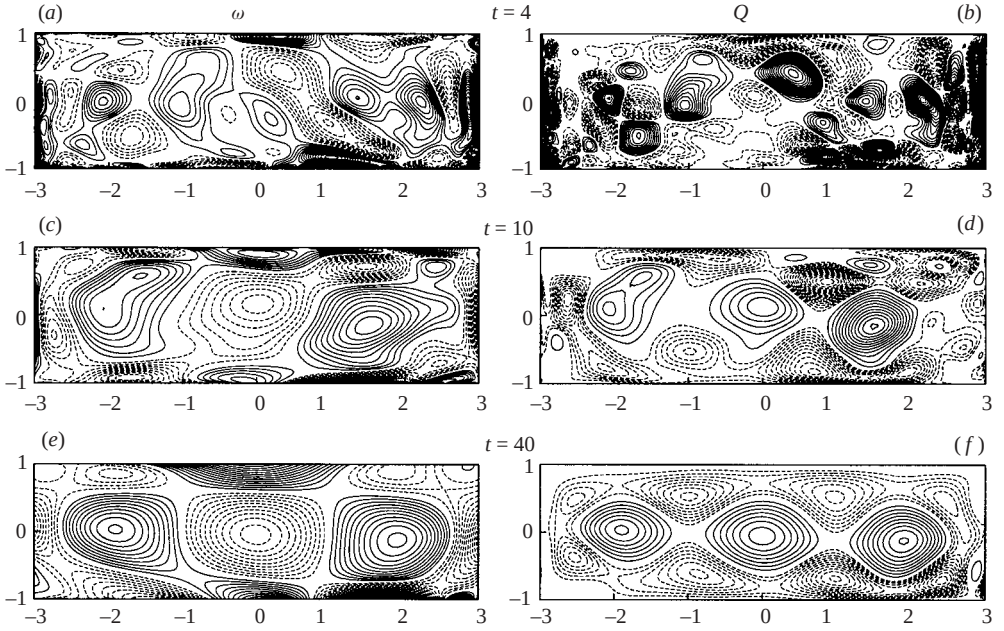

FIGURE 6. Vorticity (left column) and Weiss function (right column) contour plots of an experiment performed in a container with aspect ratio $\delta = 3$, $T_b = 0$ and $Re^* = 3000$. The contour level increment is (*a*) 0.6, (*c*) 0.2 and (*e*) 0.08 for the dashed ($\omega < 0$) and the solid ($\omega > 0$) contours, (*b*) 1, (*d*) 0.2 and (*f*) 0.05 for the dashed contours ($Q > 0$) and (*b*) 1, (*d*) 0.4 and (*f*) 0.1 for the solid contours ($Q < 0$).

the evolution. Figure 6 shows the vorticity (left column) and Weiss function (right column) contour plots for an experiment with $\delta = 3$ and $T_b = 0$. In this experiment, two dominant elongated regions of vorticity are formed in the centre of the domain at $t \simeq 4$ (figure 6*a*): one region with positive vorticity on the left and a region with negative vorticity on the right of the domain. The cores of these two vortices can be recognized as the two elliptic regions near the centre of the upper wall in figure 6(*b*). While these two vortices become more circular and move slightly more to the left (for $4 \leqslant t \leqslant 10$), a new positive vortex is formed due to merging of two smaller positive vortices on the right of the domain. Thus a pattern of three counter-rotating vortices is formed at $t \simeq 10$. Small variations in the shapes and positions of these vortices can be observed by inspection of a set of snapshots for $t > 10$, which indicate that the cell pattern is quasi-stationary. The Weiss function plots in figure 6(*d*, *f*) indicate that the elliptic cores of these three vortices are surrounded by hyperbolic regions between the vortices and the boundaries of the domain.

The biased experiment with $\delta = 3$ and $T_b = 0.09$ resulted in a large-scale motion of the fluid in a clockwise direction, superimposed on the small vortices that are formed in the wake of the moving grid. In contrast to the experiment with $\delta = 2$ shown in figure 4, this large-scale motion does not roll up into one large vortex, but it breaks up into two parts at $t \simeq 5$, forming two negative vortices at $t \simeq 10$. In our experiment with $T_b = 0.09$, the flow organizes into a quasi-stationary pattern of four counter-rotating vortices at $t \simeq 10$. The break-up of this large-scale motion is due to the detachment of vorticity from the viscous boundary layers. This wall-induced vorticity rolls up into a positive vortex which separates the two negative vortices that are formed from the large-scale motion. This decay scenario was observed in three

experiments with $\delta = 3$ and biased forcing ($T_b = 0.09$). In two experiments (with the same value of T_b), the initial large-scale motion rolled up into one central vortex, and a pattern of three counter-rotating vortices was formed.

(iii) $\delta = 4$ *and* $\delta = 5$

The influence of an initial bias becomes less important when the value of δ increases. In the case $\delta = 4$ the final flow pattern consists of five counter-rotating vortices in almost all experiments (see table 2). However, in some experiments one of the vortices was considerably smaller than the other four. The number of vortices in these experiments is denoted as $4 + 1$. In one experiment a pattern of six counter-rotating vortices is formed. In all biased experiments the net torque of the forcing was taken $T_b = 0.09$.

The streak images for experiments with $\delta = 5$ show the formation of a cell pattern consisting of five, six or seven counter-rotating vortices (see table 2). No difference was observed between experiments with and without bias in the forcing.

4. Discussion and conclusion

The laboratory experiments performed in containers with different aspect ratios δ show the self-organization of an initially disordered quasi-two-dimensional flow towards a regular quasi-steady cell pattern that fills up the whole domain. The number of vortices in these final cell patterns, N_f, depends on the aspect ratio of the flow domain, although its exact value cannot be predicted from the initial conditions. In most experiments we found $N_f = \delta$ or $N_f = \delta \pm 1$. The actual number of vortices that is formed in a particular experiment depends on the (random) position of one or two strong vortices during the intermediate stage of the flow evolution. In some experiments, a small bias was introduced to the initial flow field during the forcing ($T_b \neq 0$). This bias appeared to have a large influence on the flow evolution in containers with small aspect ratios ($\delta = 2$ or $\delta = 3$), but this influence is almost absent in containers with larger aspect ratios ($\delta = 4$ or $\delta = 5$). This observation underlines the importance of carefully performed experiments, particularly for $\delta \leqslant 3$, for the analysis and interpretation of decaying quasi-two-dimensional flows in stratified fluids in rectangular containers.

One major disadvantage of the present experiments is the relatively low effective Reynolds number of the flow (see figure 2). The strong dissipation of kinetic energy in these experiments is mainly due to vertical shearing between different layers in the stratified interface. One would expect that higher values of Re^* could be obtained by increasing the translation speed V of the forcing grid. However, experiments performed with higher values of V showed the generation of very strong and energetic internal waves. In these experiments, the kinetic energy of the quasi-two-dimensional flow in the interface appeared to be even lower than in experiments with lower values of V (in which less energy was 'lost' to internal wave generation). Therefore, it was not possible to perform experiments with higher Reynolds numbers in the present experimental configuration. Furthermore, the equipment used for quantitative flow analysis was not suitable to study small-scale details of the flow evolution. In order to obtain more detailed information about the cell pattern formation in rectangular containers, high-resolution numerical simulations were carried out on decaying two-dimensional turbulence in rectangular containers (with unbiased initial forcing). For details of the numerical method and the initialization procedure, and a discussion of the results of many runs with aspect ratio $\delta = 2$ and $\delta = 3$ we refer to Maassen (2000).

	$\delta = 2$			$\delta = 3$		
Total number of runs	19			10		
Number of vortices in final state:	1^+	2	3	3	4	?
Number of runs with $Re = 1000$:	5	4	1	3	2	0
Number of runs with $Re = 3000$:	7	1	1	3	0	2

TABLE 3. Characteristic parameters of the final states observed in numerical simulations on rectangular domains with aspect ratio δ and no-slip boundary conditions.

	$\delta = 2$		$\delta = 3$	
Number of vortices in final state:	1	2	2	3
Number of runs:	3	2	4	1

TABLE 4. Characteristic parameters of the final states observed in numerical simultions on rectangular domains with aspect ratio δ, $Re = 1000$ and stress-free boundary conditions.

The self-organization of decaying two-dimensional turbulence on a rectangular domain with no-slip boundary conditions was simulated for two different aspect ratios ($\delta = 2$ and $\delta = 3$) and two different Reynolds numbers: $Re = 1000$ and $Re = 3000$. Keeping in mind that $Re \approx 0.4Re^*$ (see § 2), the Reynolds number in the numerical experiments corresponds roughly to $Re^* \approx 2500$ and $Re^* \approx 7500$, respectively. The total number of runs for each value of δ is listed in table 3, together with the number of vortices observed in the final cell patterns and the number of runs in which this particular type of cell pattern occurs. In the case $\delta = 2$, almost all numerical runs showed the formation of a strong rotating tripolar vortex for $Re = 1000$ and $Re = 3000$. The location of this tripole is determined by the (random) position of a strong vortex core at an earlier stage in the flow evolution. A similar process occurs in the runs with $\delta = 3$, where three or four strong vortex cores dominate the flow evolution and a cell pattern of three or four counter-rotating vortices is formed. (In two of the runs with $\delta = 3$ and $Re = 3000$ the flow was dominated by small-scale structures and no clear final cell pattern was formed. This observation is indicated in table 3 by a question mark.) Similar computations have been performed with stress-free boundary conditions. These simulations showed the formation of cell patterns with a topology that differs completely from the quasi-stationary cell patterns observed in simulations with no-slip boundaries. For example, on a domain with $\delta = 2$ and stress-free boundary conditions one or two vortices are formed, each containing only one sign of vorticity. The topology of these vortices contrasts sharply with the rotating tripole observed in simulations with $\delta = 2$ and no-slip boundaries for comparable Reynolds number ($Re = 1000$). To illustrate the different decay scenarios for flows with no-slip and with stress-free boundary conditions we have shown a few vorticity contour plots from simulations with $\delta = 2$ and $Re = 1000$ in figure 7. An overview of the number of vortices in the final state of runs with stress-free boundary conditions is given in table 4.

The formation of a cell pattern of counter-rotating vortices was also predicted by maximum-entropy solutions for inviscid two-dimensional flow on a bounded rectangular domain with aspect ratio $\delta \neq 1$. Pointin & Lundgren (1976) computed the statistical equilibrium state of a system of positive and negative point vortices on a bounded rectangular domain, described by the sinh-Poisson equation $\nabla^2\psi = -\omega = -c\sinh(\beta\psi)$,

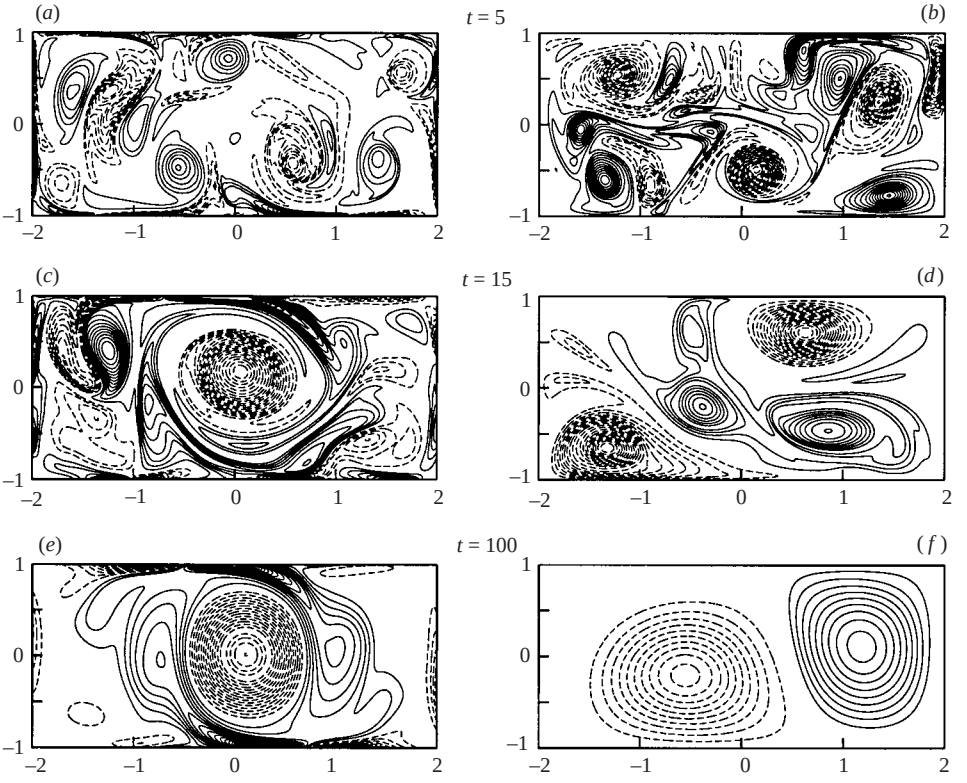

FIGURE 7. Vorticity contour plots of simulations with $\delta = 2$, $Re = 1000$ and no-slip (left column) and stress-free (right column) boundary conditions. Dashed contours represent negative values of vorticity, and solid contours represent positive values. The contour level increment is (*a*) 2, (*b*) 1, (*c*, *d*) 0.5 and (*e*, *f*) 0.2.

where the parameters c and β depend on the specific situation (see Joyce & Montgomery 1973). On a domain with aspect ratio $\delta = 2$, the solution of this equation consists of two cells of opposite circulation, that both fill one half of the domain. A similar prediction was made by Chavanis & Sommeria (1996) using a statistical mechanical theory based on patchwise discretization of the initial vorticity field. These authors found a monopolar equilibrium solution for a domain with aspect ratio $\delta < 1.12$ and a dipolar solution for a domain with $1.12 < \delta \leqslant 2$ (solutions for $\delta > 2$ were not described). Since these maximum-entropy solutions do not take into account the effects of viscous boundary layers, the structure of these cell patterns is entirely due to the rectangular geometry of the domain.

The different decay scenarios for flows with no-slip and stress-free boundaries indicate that the formation of cell patterns in laboratory experiments and numerical simulations of decaying (quasi-)two-dimensional turbulent flow in rectangular containers with no-slip boundary conditions is not merely determined by the shape of the container, but also depends significantly on the formation and detachment of viscous boundary layers. This observation is further supported by the lack of correspondence with maximum-entropy solutions for a bounded domain with $\delta = 2$, as presented by Pointin & Lundgren (1976) and Chavanis & Sommeria (1996). Such a clear disagreement between predictions from statistical-mechanical theories and numerical simulations was not found for the square container case.

One of the authors (S.R.M.) was supported by the Netherlands Geoscience Foundation (GOA) with financial aid from the Netherlands Organization for Scientific Research (NWO). Part of this work was sponsored by the Stichting Nationale Computerfaciliteiten (National Computing Facilities Foundation, NCF) for the use of supercomputer facilities, with financial support from the Nederlandse Organisatie voor Wetenschappelijk Onderzoek (Netherlands Organization for Scientific Research, NWO).

Appendix. Grid configurations

The drag force exerted on a cylindrical rod with diameter d and length l moving with constant speed V through a fluid with density ρ is given by $F_D = \frac{1}{2}C_D\rho V^2 ld$, where the appropriate value for the drag coefficient C_D is obtained from experimental data collected by Blevins (1984). Since the rods move parallel to each other and with constant speed, the angular momentum L_{rod} induced by one rod (per unit length and per unit density), defined with respect to the centre of the domain, is proportional to the torque T exerted by this force:

$$L_{rod} = \frac{1}{\rho l}\int_0^\tau T\,\mathrm{d}t = \frac{F_D y\tau}{\rho l} = \frac{F_D ya}{\rho lV} = \frac{1}{2}C_D V yad, \tag{A 1}$$

where t is the time and τ the time duration of the forcing, and a the total displacement of the rods ($a = \tau V$). The grid configurations used in the laboratory experiments are specified by means of the y-coordinates y_i of the rods (in cm), see figure 1. The net angular momentum L_0 induced on the flow can be calculated from these y-coordinates by using the expression: $L_0 = \sum_{i=1}^{P} L_i = \frac{1}{2}C_D V ad \sum_{i=1}^{P} y_i$, with P the number of rods. The 'bias' T_b induced in the initial forcing can be calculated by means of equation (3.1).

The five grid configurations used are:
Grid R1: ($\pm$18, $\pm$17, $\pm$10, $\pm$9, $\pm$8, $\pm$1, 0)
Grid R2: ($\pm$18, $\pm$16, $\pm$14, $\pm$12, $\pm$3, $\pm$1)
Grid R3: ($\pm$17, $\pm$15, $\pm$13, $\pm$11, $\pm$3, $\pm$1)
Grid R4: ($-$19, 18, 14, $-$12, 10, 6, $-$5, 2)
Grid R5: ($-$19, 17, $\pm$12, 7, $-$5, 2)

REFERENCES

Blevins, R. D. 1984 *Applied Fluid Dynamics Handbook*. Van Nostrand Reinhold.

Chavanis, P. H. & Sommeria, J. 1996 Classification of self-organized structures in two-dimensional turbulence: the case of a bounded domain. *J. Fluid Mech.* **314**, 267–297.

Clercx, H. J. H., Maassen, S. R. & van Heijst, G. J. F. 1998 Spontaneous spin-up during the decay of 2D turbulence in a square container with rigid boundaries. *Phys. Rev. Lett.* **80**, 5129–5132.

Clercx, H. J. H., Maassen, S. R. & van Heijst, G. J. F. 1999 Decaying two-dimensional turbulence in square containers with no-slip or stress-free boundaries. *Phys. Fluids* **11**, 611–626.

Fincham, A. M., Maxworthy, T. & Spedding, G. R. 1996 Energy dissipation and vortex structure in freely decaying, stratified grid turbulence. *Dyn. Atmos. Oceans* **23**, 155–169.

Flór, J. B. 1994 Coherent vortex structures in stratified fluids. PhD thesis, Eindhoven University of Technology.

van Heijst, G. J. F., Davies, P. A. & Davis, R. G. 1990 Spin-up in a rectangular container. *Phys. Fluids* A **2**, 150–159.

Joyce, G. & Montgomery, D. 1973 Negative temperature states for the two-dimensional guiding centre plasma. *J. Plasma Phys.* **10**, 107–121.

van de Konijnenberg, J. A., Andersson, H. I., Billdal, J. T. & van Heijst, G. J. F. 1994 Spin-up in a rectangular tank with low angular velocity. *Phys. Fluids* **6**, 1168–1176.

Li, S. & Montgomery, D. 1996 Decaying two-dimensional turbulence with rigid walls. *Phys. Lett.* A **218**, 281–291.

Li, S., Montgomery, D. & Jones, W. B. 1996 Inverse cascades of angular momentum. *J. Plasma Phys.* **56**, 615–639.

Li, S., Montgomery, D. & Jones, W. B. 1997 Two-dimensional turbulence with rigid circular walls. *Theor. Comput. Fluid Dyn.* **9**, 167–181.

Lilly, D. K. 1983 Stratified turbulence and the mesoscale variability of the atmosphere. *J. Atmos. Sci.* **40**, 749–761.

Maassen, S. R. 2000 Self-organization of confined two-dimensional flows. PhD thesis, Eindhoven University of Technology.

Maassen, S. R., Clercx, H. J. H. & van Heijst, G. J. F. 2002 Self-organization of quasi-2D turbulence in stratified fluids in square and circular containers. *Phys. Fluids* **14**, 2150–2169.

Nguyen Duc, J.-M. & Sommeria, J. 1988 Experimental characterization of steady two-dimensional vortex couples. *J. Fluid Mech.* **192**, 175–192.

Pointin, Y. B. & Lundgren, T. S. 1976 Statistical mechanics of two-dimensional vortices in a bounded container. *Phys. Fluids* **19**, 1459–1470.

Riley, J. J. & Lelong, M.-P. 2000 Fluid motions in the presence of strong stable stratification. *Annu. Rev. Fluid Mech.* **32**, 613–657.

Riley, J. J., Metcalfe, R. W. & Weissman, M. A. 1981 Direct numerical simulations of homogeneous turbulence in density stratified fluids. *Proc. AIP Conf. Nonlinear Properties of Internal Waves* (ed. B. J. West), pp. 79–112.

Weiss, J. 1981 The dynamics of enstrophy transfer in two-dimensional hydrodynamics. *Tech. Rep.* LJ1-TN-81-121. La Jolla Institute.

Yap, C. T. & Van Atta, C. W. 1993 Experimental studies of the development of quasi-two-dimensional turbulence in stably stratified fluid. *Dyn. Atmos. Oceans* **19**, 289–323.